JSME Int. J., Vol. 47, No. 3, Ser. B, pp. 522-527, (2004)

Development of Micro Catalytic Combustor with Pt/Al_2O_3 Thin Films

Yuji SUZUKI, Joichi SAITO, and Nobuhide KASAGI

Department of Mechanical Engineering, The University of Tokyo
7-3-1, Hongo, Bunkyo-ku, Tokyo 113-8656, JAPAN

e-mail: ysuzuki@thtlab.t.u-tokyo.ac.jp

Key Words: Catalytic combustor, anodic oxidation, Pt/Al_2O_3 catalyst, MEMS

ABSTRACT

Catalytic combustion of butane in micro-scale conduits is investigated. Nano-porous alumina formed through anodic oxidation of aluminum is employed for the support of platinum catalyst. Combustion starts at 250 ˚C, and a heat release rate up to 710MW/m^3 is achieved in a 0.6mm ID tube. It is found that the surface reaction speed is a limiting factor for the overall reaction rate. A prototype silicon-based catalytic combustor is designed and fabricated using MEMS technologies. The Pt/alumina catalyst layer is successfully integrated onto a silicon microchannel, and a Pyrex lid is anodically bonded onto the Si substrate. It is found in a preliminary experiment that the MEMS combustor also works well, but gives somewhat smaller reaction rate due to the thinner catalytic layer.

INTRODUCTION

Due to recent advances of mobile electronic devices such as laptop computers and cellular phones, the worldwide demand for primary and secondary batteries is growing 6% annually[1]. Li-ion battery has the highest energy density among secondary batteries for consumer use, but its energy density is projected to reach only 300Wh/kg. On the other hand, the energy density of hydrocarbon fuel such as butane and methanol is by more than two orders of magnitudes lager. Therefore, local power generation of only a few percent conversion efficiency may provide much higher energy density than batteries.

Recently, portable power generation systems of various kinds such as MEMS gas turbine[2], micro rotary IC engine[3], micro fuel cell[4], and micro thermoelectric power generator[5] are under development. However, each system has its own challenges or drawbacks as well as advantages. Therefore, no single system is currently considered to prevail the others in real applications.

The final goal of the present study is to develop an external combustion engine such as micro steam engine or micro Stirling engine[6]. In these systems, combustion in small scale is one of the most important technological issues. For hydrocarbon fuels, reaction speed is much slower than hydrogen and quenching should occur in sub-millimeter scale. Therefore, heterogenous catalytic combustion rather than homogeneous gas phase reaction is preferred[7-11].

Sitzki et al.[7] developed so-called Swiss-roll combustors having a counter flow heat exchanger lapping around the combustion region in order to reduce heat loss to ambient. They employed a bulk Pt wire as the catalyst and found that combustion starts at lower temperature. Wang et al.[8] developed a micro ceramic combustor with a tape-casting method, and measured reaction rate of *n*-butane at low equivalence ratios on Pd/alumina catalysts. Arana et al.[9] fabricated suspended-tube reactor, which could significantly reduce heat loss and maintain temperature gradient of up to 2000 ˚C/mm. They report that catalytic ammonia cracking leading to 1.6 W of hydrogen can be made. Spadaccini et al.[10] developed a prototype catalytic combustor for the MEMS gas turbine. They employed platinum coated form as the catalyst insert and obtained 60-70% combustion efficiency for hydrogen, but the efficiency was decreased to 10-30% for propane and ethylene near the stoichiometry condition due to its slower reaction speed. Splinter et al.[11] employed 70μm-thick porous silicon as their Pd catalyst support and developed a micro membrane reactor. They showed that oxidation of CO was successfully made in their reactor. The previous studies described above employ conventional washcoat or sol-gel methods to prepare the catalyst layer. However, it is not straightforward to integrate those catalyst layers into micro channels.

The objectives of the present study are to develop micro catalytic combustor with anodized alumina support and to evaluate its performance in a series of laboratory experiments. The advantages of the anodized alumina support are three folds; firstly, unlike conventional washcoat process, it is easy to control the support thickness

and its characteristics such as porosity. Secondly, adhesion between alumina and aluminum is good, so that the catalyst layer is free from thermal shock possibly occurring in micro combustors. Thirdly, once aluminum layer is formed, it is easy to oxidize it into alumina through anodic oxidation even in complex geometry.

CATALYST LAYER

Figure 1 shows schematically an anodic oxidation bath, in which a 4 wt% oxalic acid solution is employed. The temperature of the solution is kept at 10 ˚C by an external water loop. A constant current source and stainless steel plate are respectively employed for the power supply and the cathode. After the oxidation followed by a bake at 350 ˚C for 1 hour, porous alumina is formed on the anode surface (Fig. 2). Then, the sample is submerged into diammine dinitro platinum (II) solution, and calcinated at 350˚C for 1 hour to make platinum impregnated into the nano-porous alumina layer.

Figure 3 shows SEM images of the alumina layer fabricated with a current density I_A of 50 A/m^2. Honeycomb-like pore structures can been seen, although the pore diameter and the distance between pores are not uniformly distributed. The pore characteristics of the alumina and its thickness depend on the current density and the oxidation duration[12, 13]. In the present study, 5 μm-thick alumina is obtained with anodization for 50 minutes. Figure 4 shows pore diameter distribution measured with a mercury porosimeter. The mean diameter of the pore is about 20-30 nm, which is in agreement with the result of Sungkono et al. [13]. The distance between neighboring nanopores is about 90nm, which corresponds to the surface area of 2.1 m^2/g. After calcination, the surface area is markedly increased to 100-200 m^2/g[13].

After impregnation of Pt, the catalyst layer is examined with X-ray fluorescent analysis in order to confirm presence of Pt. Contents of Pt in the alumina layer is designed to be around 1 wt%, although it is not directly measured in the present study.

COMBUSTION EXPERIMENT IN MICRO TUBE

In our first stage, a catalytic layer is formed inside 0.6 mm ID aluminum tube and the combustion characteristic is measured systematically. The outer diameter and the length of the tube is 1 mm and 50 mm, respectively.

Figure 5 shows a schematic of the present experimental setup. Air and *n*-butane are supplied from gas cylinders. Their flow rates are separately measured by thermal mass flow meters (Oval Corp., MASFLO). Then, the fluids are mixed and introduced into the test section. Combustion experiment is made in a solder bath, by which the solder temperature can be maintained constant between 190 and 400 ˚C. Due to the high thermal conductivity and large heat capacity of solder, the combustion tube temperature can be kept constant almost independently of the amount of heat generation at the catalyst layer. The true temperature of the catalyst

layer is estimated with the inlet and outlet gas temperatures assuming that the heat transfer coefficient at the tube inner wall can be given by its theoretical value of the laminar forced convection.

A gas analyzer (TSI Inc., CA-6215) is employed to measure concentration of O_2, CO_2 and NOx in the exhaust gas. The reaction rate is calculated from the O_2 concentration at the exit. Under the present experimental condition, the equivalent ratio is kept unity and the flow rate Q of *n*-butane is changed between 2.5 - 25 sccm, which corresponds to heat generation of 5 - 50 W if 100% reaction is achieved. The Reynolds number is less than 20 in all experimental conditions examined. Therefore, the velocity and thermal entrance lengths are less than the tube diameter, and their effect should be minor.

Figure 6 shows the reaction heat in the combustion tube anodized with I_A = 50 A/m^2 for 12 hours. The alumina thickness is estimated to be 35 μm in this case. The onset of combustion is around 250 ˚C and the heat generated is increased with the catalyst temperature. At 400 ˚C, 100% reaction is achieved at the flow rate of 5 sccm, while the maximum heat generation is 32 W at 450 ˚C for Q = 25 sccm. Therefore, heat generation density for 100% conversion is as large as 710 MW/m^3, which is one-order of magnitude larger that of the industrial gas turbine combustors.

As shown in Fig. 7, the concentration of CO is almost zero for Q = 5 sccm. But, it becomes appreciable for Q > 5 sccm, where 100% conversion is not achieved. Note that NOx concentration is always less than 1 ppm within the measurement accuracy of the gas analyzer presently used..

NUMERICAL ANALYSIS USING 1-D PLUG FLOW MODEL

In macro-scale catalytic combustors, diffusion in the bulk fluid is the major limiting factor, and the heat generation density is generally lower than homogenous well-stirred combustors. On the other hand, the micro catalytic combustor presently developed has very large heat generation density even at low catalyst temperature as shown in Fig. 6. In this section, we make a curve fitting of our experimental data to a simple plug flow model in order to clarify the limiting factor for the overall reaction.

In the present analysis, we made the following assumption for simplicity:

i) single surface reaction with Arrhenius type, i.e.,

$$C_4H_{10} + 6.5O_2 \rightarrow 4CO_2 + 5H_2O, \tag{1}$$

ii) constant physical and thermal properties,

iii) infinite diffusion rate in the porous catalyst support.

Then, the conservation of mass is written as,

$$A_c \frac{d\, U_m C_{B,b}}{dx} + W_p R_B = 0, \tag{2}$$

where A_c, U_m, $C_{B,b}$, W_p, and R are respectively the cross-sectional area, the bulk mean velocity, the mole concentration of butane in the bulk fluid, wetted area per unit streamwise length, and the reaction rate. The first-order rate equation is given by,

$$R_B = C_{B,s} \cdot A \exp\left(-\frac{E}{R_g T} \right), \tag{3}$$

where $C_{B,s}$ is the mole concentration of butane at the wall surface. The quantity A is a pre-exponential factor, which includes the effect of the true reaction area and the effectiveness factor of the catalyst, while E and R_g denote the activation energy, and the universal gas constant, respectively. Strictly speaking, Eq. (3) is only valid in the presence of a large excess of oxygen [14]. In the present stoichiometry condition, however, the concentration of oxygen might also be included in Eq. (3). But, as far as the authors' knowledge, the rate equation for butane is not available near the stoichiometry condition. Therefore, we keep Eq. (3) for our preliminary analysis to obtain a zeroth-order analytical result. Since the catalyst temperature T is kept constant in the present experiment, T is independent of the streamwise location x.

Mole balance equation between the surface reaction and the molecular diffusion of butane to the wall surface can be given by

$$R_B = k_B \left(C_{B,b} - C_{B,s} \right), \tag{4}$$

where k_B is the mass transfer rate of butane. By combining Eqs. (2)-(4), we get,

$$A_c \frac{d\, U_m C_{B,b}}{dx} = -\frac{W_p k_B A \exp\left(-E / R_g T\right)}{k_B + A \exp\left(-E / R_g T\right)} C_{B,b}. \tag{5}$$

Since total mole concentration is within 4.5% difference between before and after the combustion, we further neglect the streamwise change of the bulk mean velocity. Thus, the solution of Eq. (5) is given by,

$$C_{B,b}(x) = C_{B,b}(0) \exp\left\{ -\frac{W_p k_B}{U_m A_c} \cdot \frac{A \exp\left(-\frac{E}{R_g T} \right)}{k_B + A \exp\left(-\frac{E}{R_g T} \right)} x \right\}. \tag{6}$$

Since the flow in the combustion tube is in the laminar flow range, the Sherwood number is assumed to be constant. Then, k_B can be given by

$$k_B = Sh \cdot \frac{D_B}{d} \sim 4\frac{D_B}{d}, \tag{7}$$

where D_B and d are the binary diffusion rate of butane in air and the tube inner diameter. Since the mole concentration of butane at the stoichiometry condition is as low as 3%, D_B is independent on the butane concentration. Temperature dependance of the diffusion rate is given by $D_B \propto T^{1.833}$.

A least-square method is used to determine two unknown parameters in Eq. (6), i.e., E, and A, which should strongly depend on the fabrication process of the catalyst layer. By fitted to the experimental data for Q=5 sccm, we get E=2.12x10^7 [J/mol] and A=1.79x10^3 [mol m/s]. As shown in Fig. 8, the present simple model using the same set of E and A exhibits similar trends with the experimental data for Q = 2.5, 5, 15 sccm. It is also found from this set of E and A that the mass transfer coefficient k_B is at least one order of magnitude larger than the reaction speed $A\exp(-E/R_gT)$. Therefore, in the present small-diameter tube, molecular diffusion in fluid is no more the limiting factor, and the surface reaction speed itself should play a dominant role in determining the overall reaction rate. We should have potential to increase the overall reaction rate by optimizing the fabrication process of the catalyst layer.

MEMS CATALYTIC COMBUSTOR

Experimental data shown above encourage us to develop micro catalytic combustor with the aid of MEMS technologies.

Figure 9 shows a schematic of Si-based catalytic combustor. Trapezoidal channels are formed into the Si substrate using anisotropic etching of (100) Si wafer. The surface area of the Pt/alumina catalyst layer is chosen as the same as that of the 0.6mm ID tube shown in the previous chapter. Hydraulic diameter of each channel is 261μm.

Fabrication process shown in Fig. 10 starts with a 3" Si wafer having thermally-grown 0.5μm-thick SiO_2 layers. Firstly, the oxide layer is patterned with BHF for the channel and the fluid ports, followed by anisotropic etching with TMAH (Fig. 10a). The oxide mask layer is then removed with BHF and a 2nd oxide layer is formed using wet oxidation for an electrical insulation layer (Fig. 10c). Aluminum film having 5 μm in thickness is then deposited with a thermal evaporator and patterned in such a way that aluminum remains only inside the channel (Fig. 10e). The aluminum film is transformed into nano-porous alumina using anodic oxidation as described above. Finally, a Pyrex glass wafer is anodically bonded to the Si wafer and Pt is impregnated. Due

to poor adhesion between the thermally-deposited aluminum film and SiO_2, the thickness of the catalyst layer is limited to 5 μm due to large residual stress inside the aluminum film. Note that thicker films can be made when stress control of the aluminum film is carefully carried out.

Figure 11 shows a top view of the Si-based catalytic combustor having 8 parallel channels and two fluidic ports. In our preliminary experiment, polyimide tube is attached on the top of the ports using high-temperature glue. We also tried to use anodic bonding between a Fe-Ni-Co alloy manifold and the Pyrex lid, but the glass is cracked due to slight mismatch of the temperature coefficients of expansion. Figure 12 shows the reaction heat versus the catalyst temperature. About 15 W combustion is achieved, where the reaction rate is remained below 60%. This is partially because of the thinner catalyst layer than that used in the tube experiment. It is also noted that the design of the manifold is not optimize to get uniform flow rate for the multiple channels. Anisotropic etch of the Si substrate for making the channels hinders flexible arrangement of the manifold.

CONCLUSIONS

Micro catalytic combustion of butane using anodized nano-porous alumina support is investigated. It is found in combustion experiments using 0.6mm ID tube that combustion starts at 250 ˚C, and a heat release rate up to 710 MW/m^3 is achieved. It is shown through the curve fitting of the experimental data to a 1-D plug flow model that the surface reaction is the bottle neck of the overall reaction. A silicon-based catalytic combustor with embedded Pt/alumina catalyst layer is designed and its prototype is successfully fabricated using MEMS technologies. The MEMS combustor also works reasonably well in a preliminary experiment, but gives somewhat smaller reaction rate.

ACKNOWLEDGMENT

The authors are grateful to Mr. Y. Horii for his cooperation in the experiment. This work was supported through the Grant-in-Aid for Young Scientists A (No. 14702028) by the Ministry of Education, Science, Culture and Sports (MEXT).

REFERENCES

[1] Freedonia Industry Study, World batteries, (2002).

[2] Epstein, A. H., Senturia, S. D., Al-Midani, O., Anathasuresh, G., Ayon, A., Breuer, K., Chen, K.-S., Ehrich, F. E., Esteve, E., Frechette, L., Gauba, G., Ghodssi, R., Groshenry, C., Jacobson, S., Kerrebrock, J. L., Lang, J. H., Lin, C.-C., London, A., Lopata, J., Mehra, A., Mur Miranda, J. O., Nagle, S., Orr, D. J., Piekos, E., Schmidt, M. A., Shirley, G., Spearing, S. M., Tan, C. S., Tzeng, Y.-S., and Waitz. I. A., "Micro-heat engines, gas turbines, and rocket engines - the MIT microengine project-," 28th AIAA Paper 97-1773, (1997), pp. 1-12.

[3] Fernandez-Pello, A. C., Fu, K., Knobloch, A.J., Martinez, F. C., Walther, D. C., Pisano, A. P., Liepmann, D., Maruta K., and Miyasaka, K., "Design and Experimental Results of Small-Scale Rotary Engines," Proc. 2001 Int. Mechanical Engineering Congr. and Expo. (IMECE), ASME publication IMECE/MEMS-23924, (2001).

[4] Palo, D. R., Holladay, J. D., Rozmiarek, R. T., Guzman-Leong, C. E., Wang, Y., Hu, J., Chin, Y.-H., Dagle, A., and Baker, E. G., "Development of a soldier-portable fuel cell power system Part I: A bread-board methanol fuel processor," J. Power Sources, **108**, (2002), pp. 28-34.

[5] Schaevitz, S., Franz, A. J., Jensen, K. F., and Schmidt, M. A., "A combustion-based MEMS thermoelectric power generator," Proc. 11th Int. Conf. on Solid-State Sensors and Actuators, Munich, Germany, (2001), pp. 30-33.

[6] Fukui, T., Shiraishi, T., Murakami, T., and Nakajima, N., "Study on high specific power micro-Stirling engine," JSME Int. J., Ser. B., **42**, (1999), pp. 776-782.

[7] Sitzki, L., Borer, K., Wussow, S., Schuster, E., Ronney, P. D., and Cohen, A., "Combustion in microscale heat-recirculating burners," AIAA paper, 2001-1087, (2001).

[8] Wang, X., Zhu, J., Bau, H., and Gorte, R. J., "Fabrication of micro-reactors using tape-casting methods," Catalysis Lett., **77**, (2001), pp. 173-176.

[9] Arana, L. R., Schaevitz, S. B., Franz, A. J., Schmidt, M. A., and Jensen, K. F., "A microfabricated suspended-tube chemical reactor for fuel processing," J. MEMS, **12**, (2003), pp. 600-612.

[10] Spadaccini, C. M., Zhang, X., Cadou, C. P., Miki, N., and Waitz, I. A., "Preliminary development of a hydrocarbon-fueled catalytic micro-combustor," Sensors Actuators, A, **103**, (2003), pp. 219-224.

[11] Splinter, A., Sturmann, J., Bartels, O., and Benecke, W., "Micro membrane reactor: a flow-through membrane for gas pre-combustion," Sensors Actuators, B, **83**, (2002), pp. 169-174.

[12] Sulka, G. D., Stroobants, S., Moshchalkov, V., Borghs, G., and Celis, J.-P., "Symthesis of well-ordered nanopores by anodizing aluminum foils in sulfuric acid," J. Electrochem. Soc., **149**, (2002), D97-D103.

[13] Sungkono, I. E., Kameyama, H., and Koya, T., "Development of catalytic combustion technology of VOC materials by anodic oxidation catalyst," Appl. Surf. Sci., **121/122**, (1997), pp. 425-428.

[14] Rader, C. G., and Weller, S. W., "Ignition on catalytic wires: kinetic parameter determination by the heated-wore technique," AIChE J., **20**, (1974), pp. 515-522.

Figure list

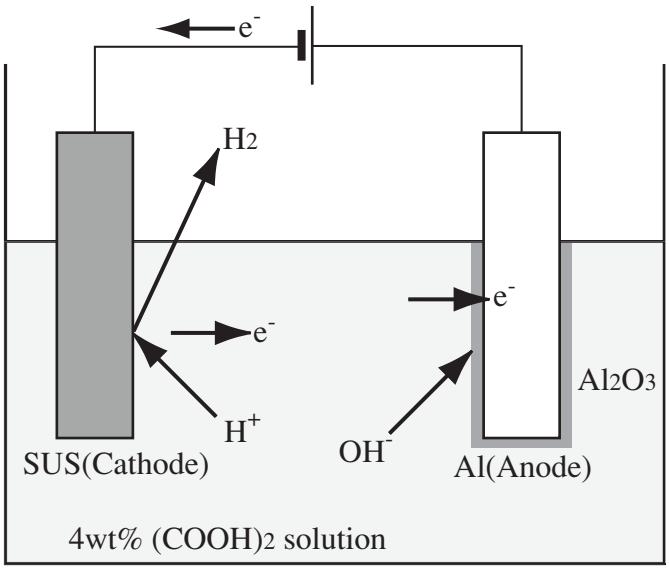

Figure 1 Schematic of anodic oxidation bath.

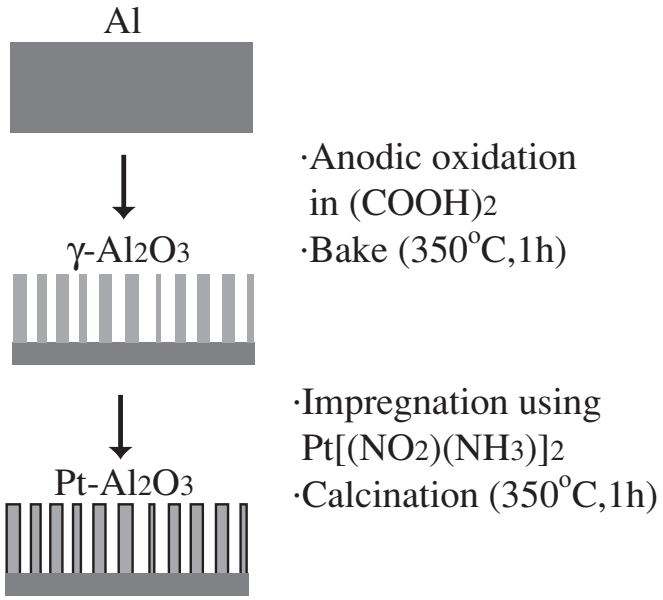

Figure 2 Fabrication process for Pt catalyst on nano-porous alumina support.

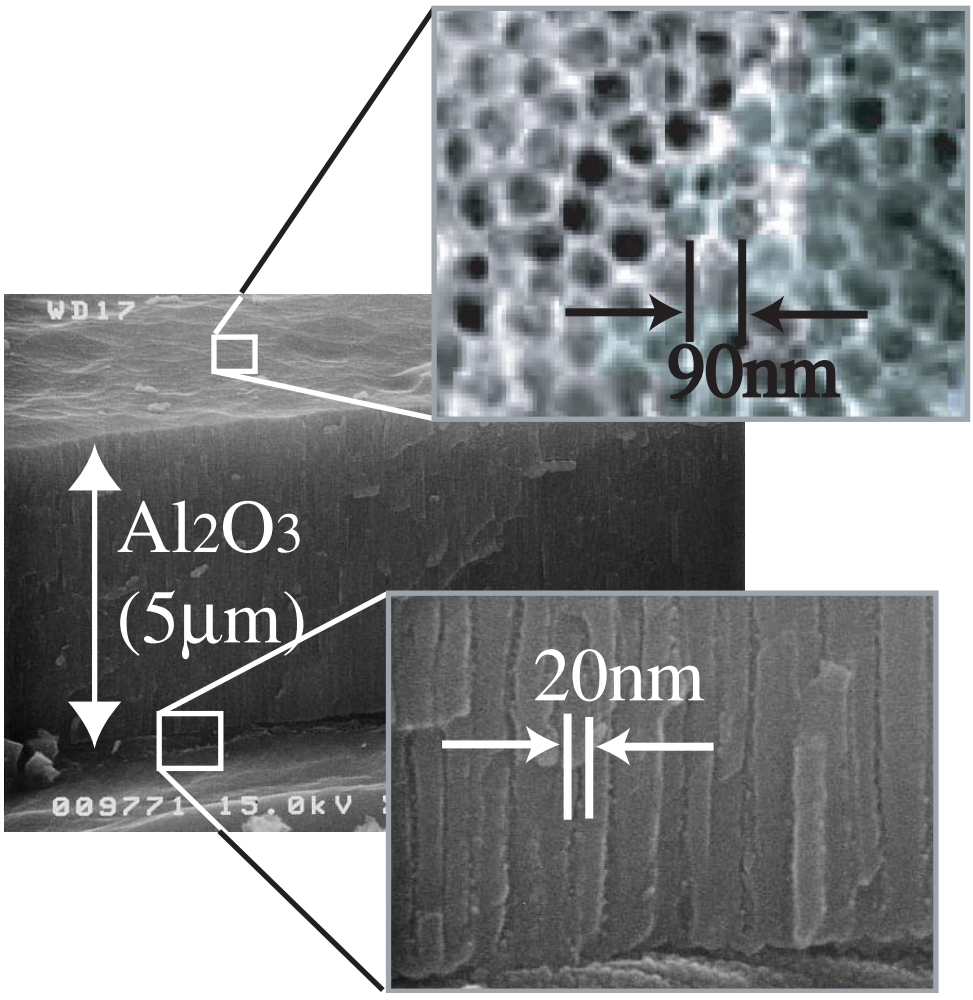

Figure 3 SEM images of porous alumina layer made by anodic oxidation at I_A=50 A/m^2.

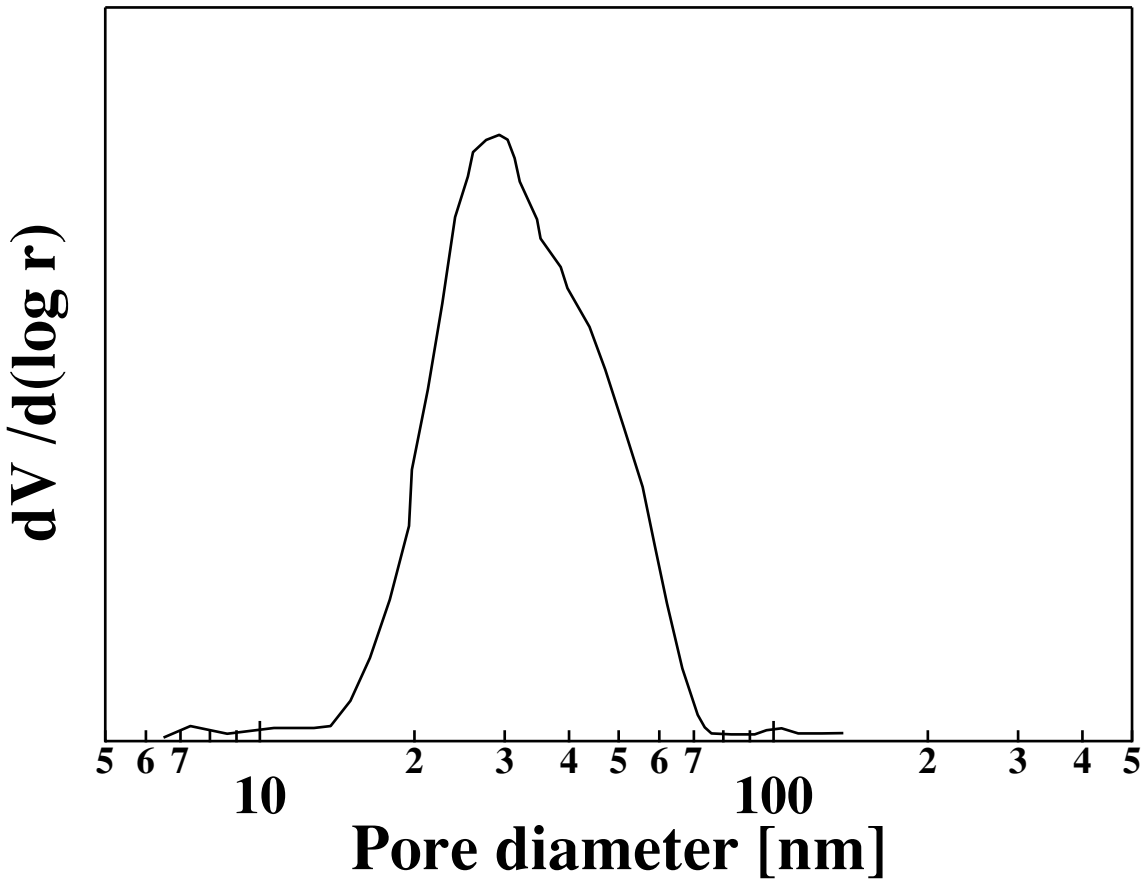

Figure 4 Pore diameter distribution.

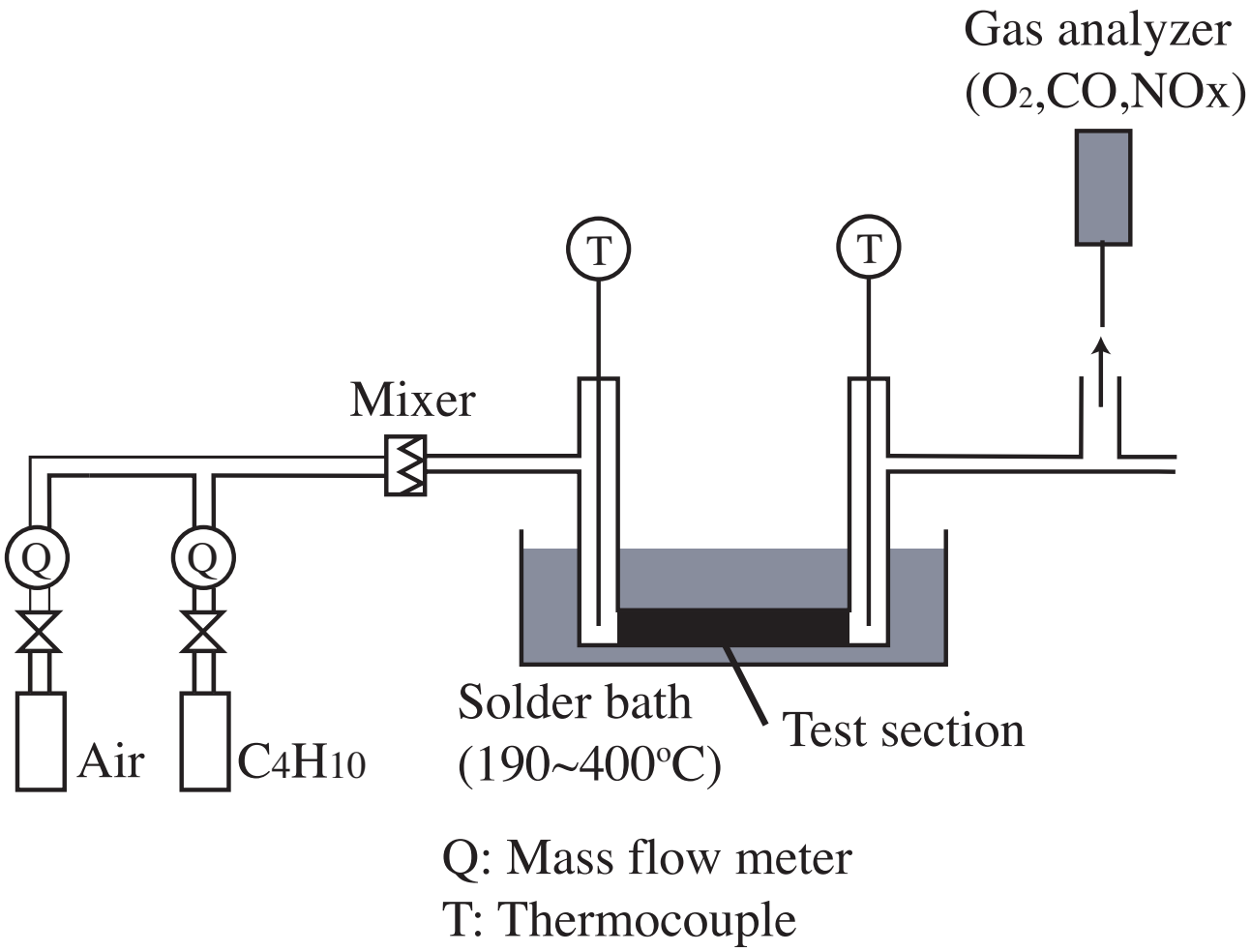

Figure 5 Experimental setup.

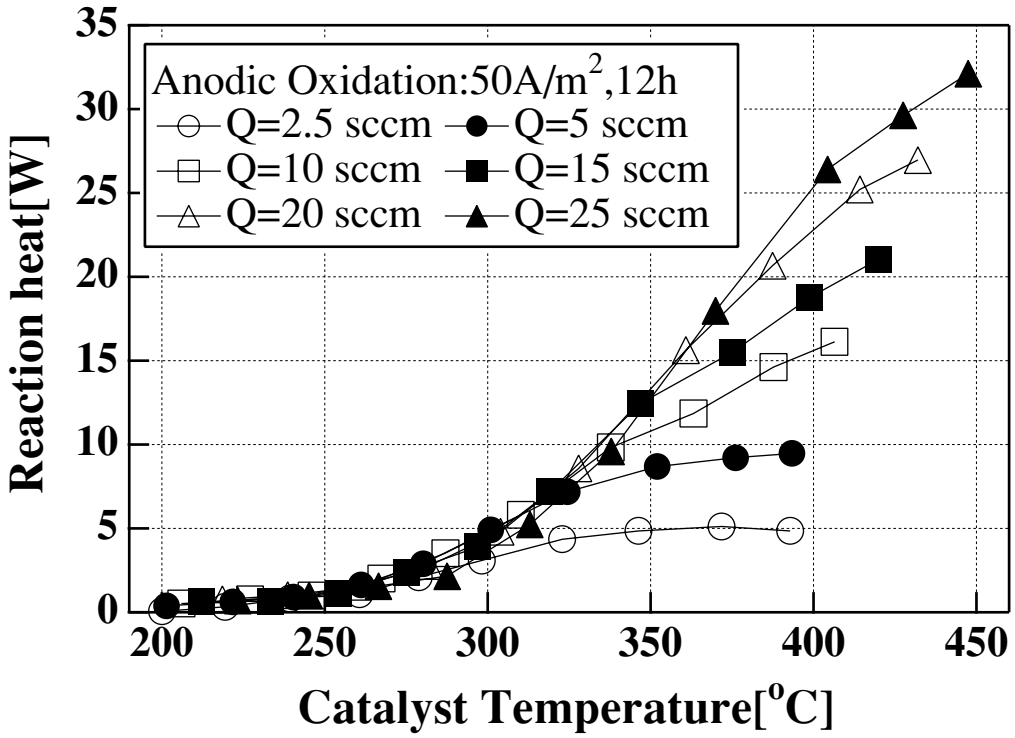

Figure 6 Reaction heat in 0.6mm ID tube with Pt/Al_2O_3 catalyst .

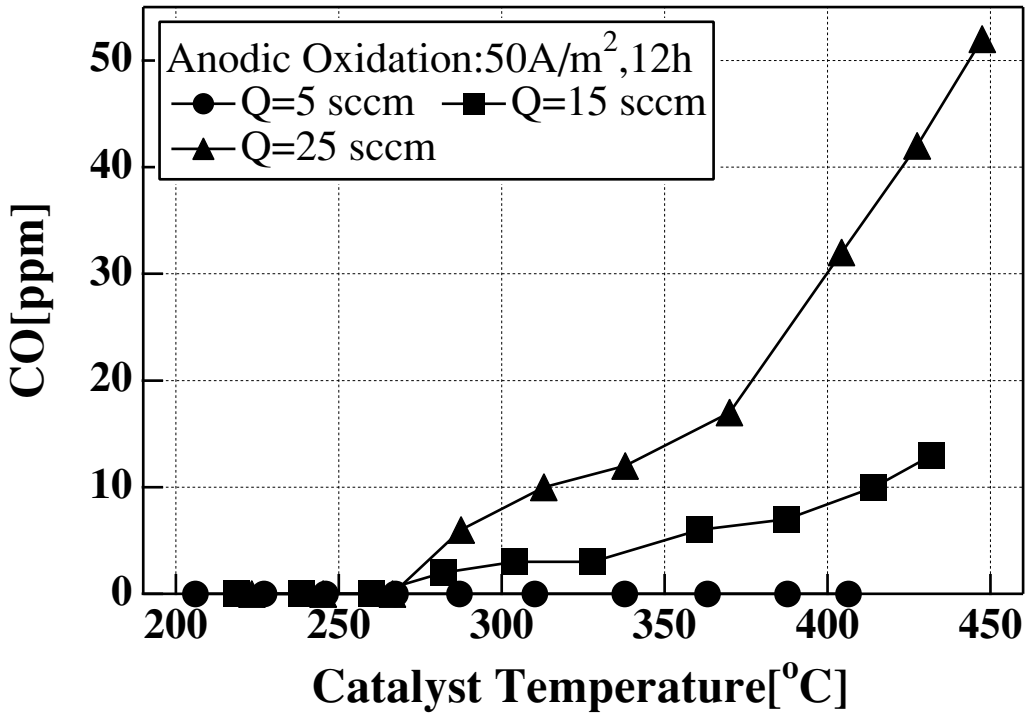

Figure 7 CO concentration in 0.6mm ID tube with Pt/Al_2O_3 catalyst .

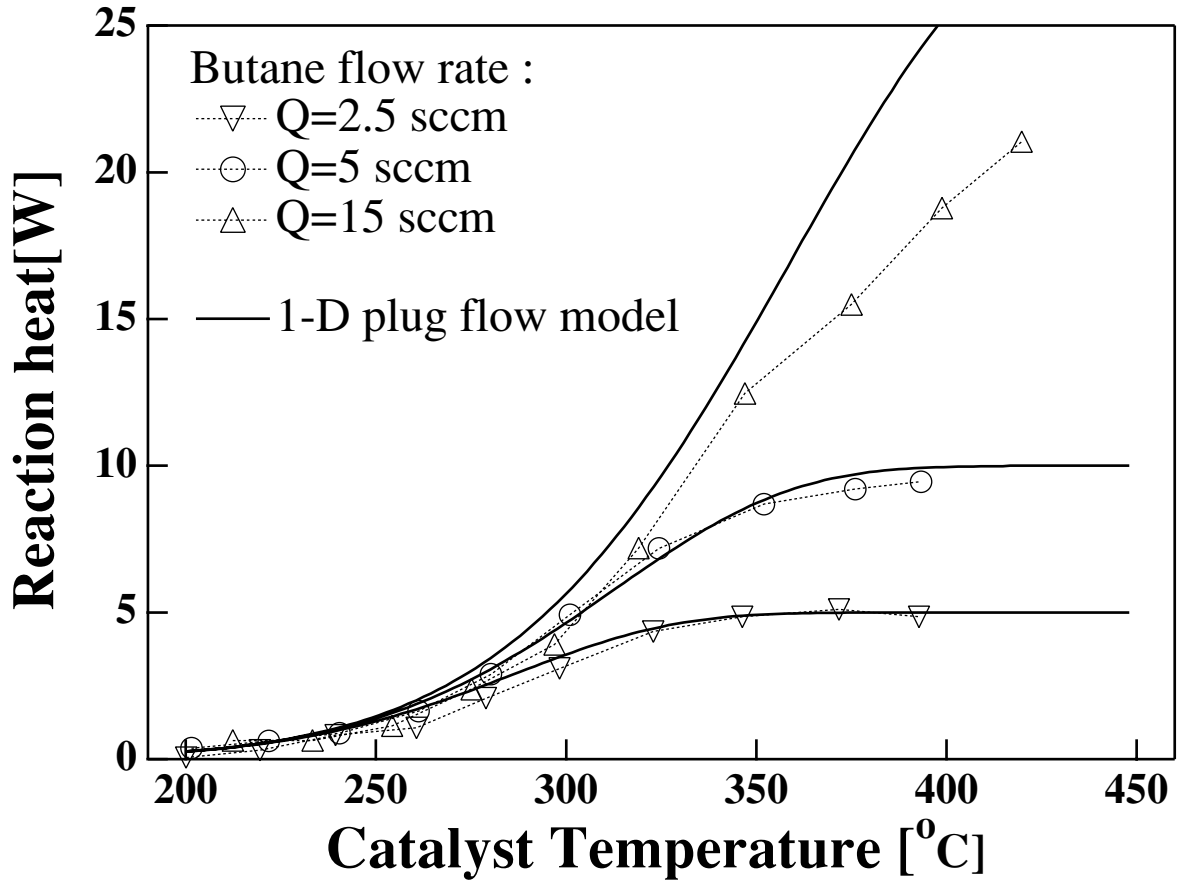

Figure 8 Comparison between 1-D plug flow model prediction and the present experimental data.

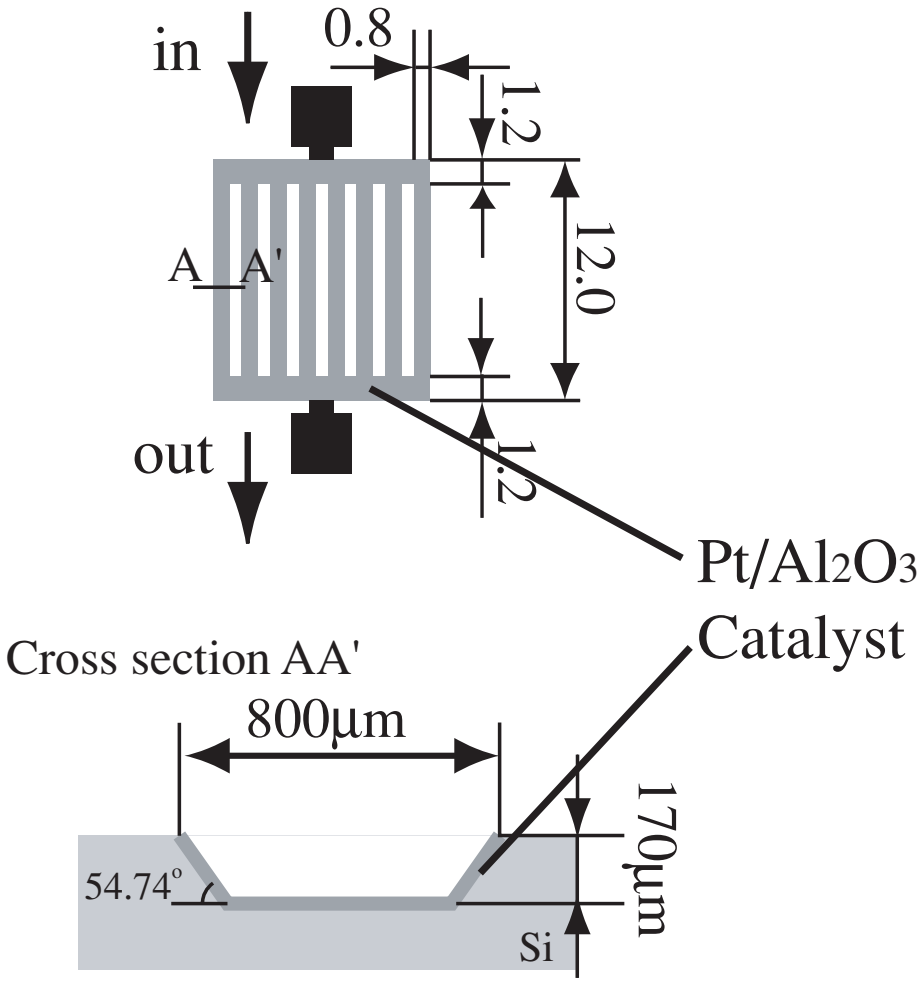

Figure 9 Schematic of micro catalytic combustor on Si substrate.

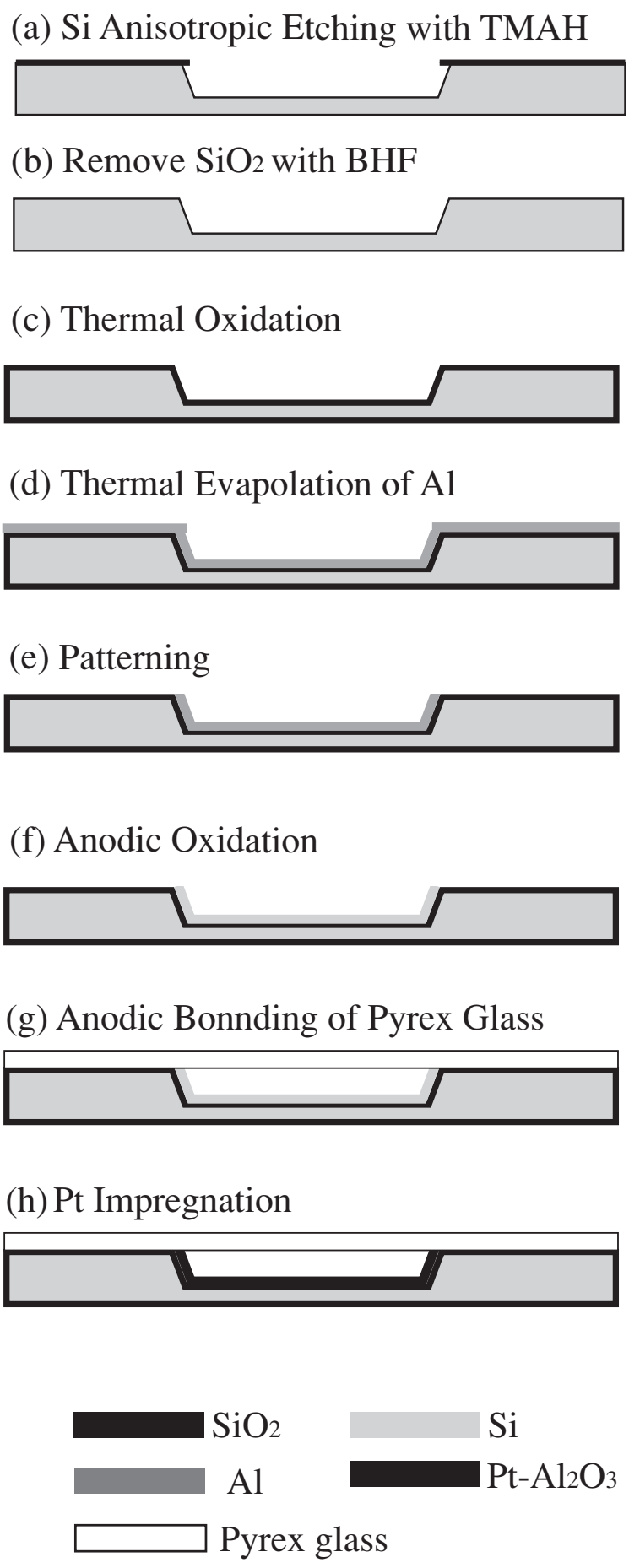

Figure 10 Process flow of Si-based micro catalytic combustor.

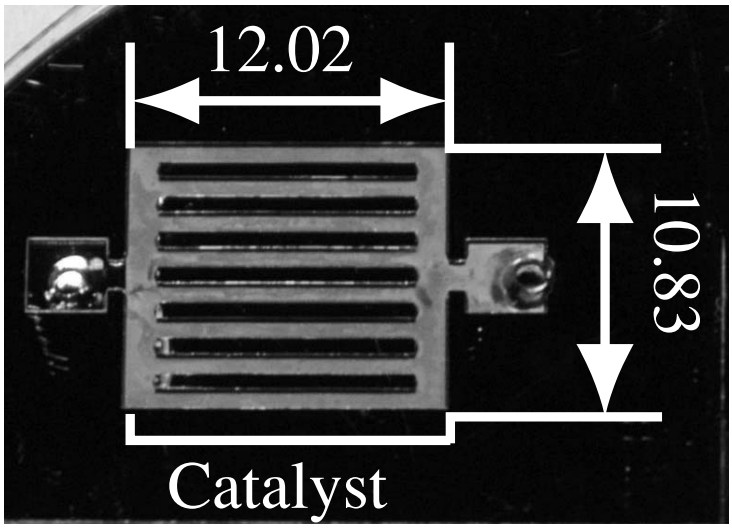

Figure 11 Prototype of Si-based micro catalytic combustor (units: mm).

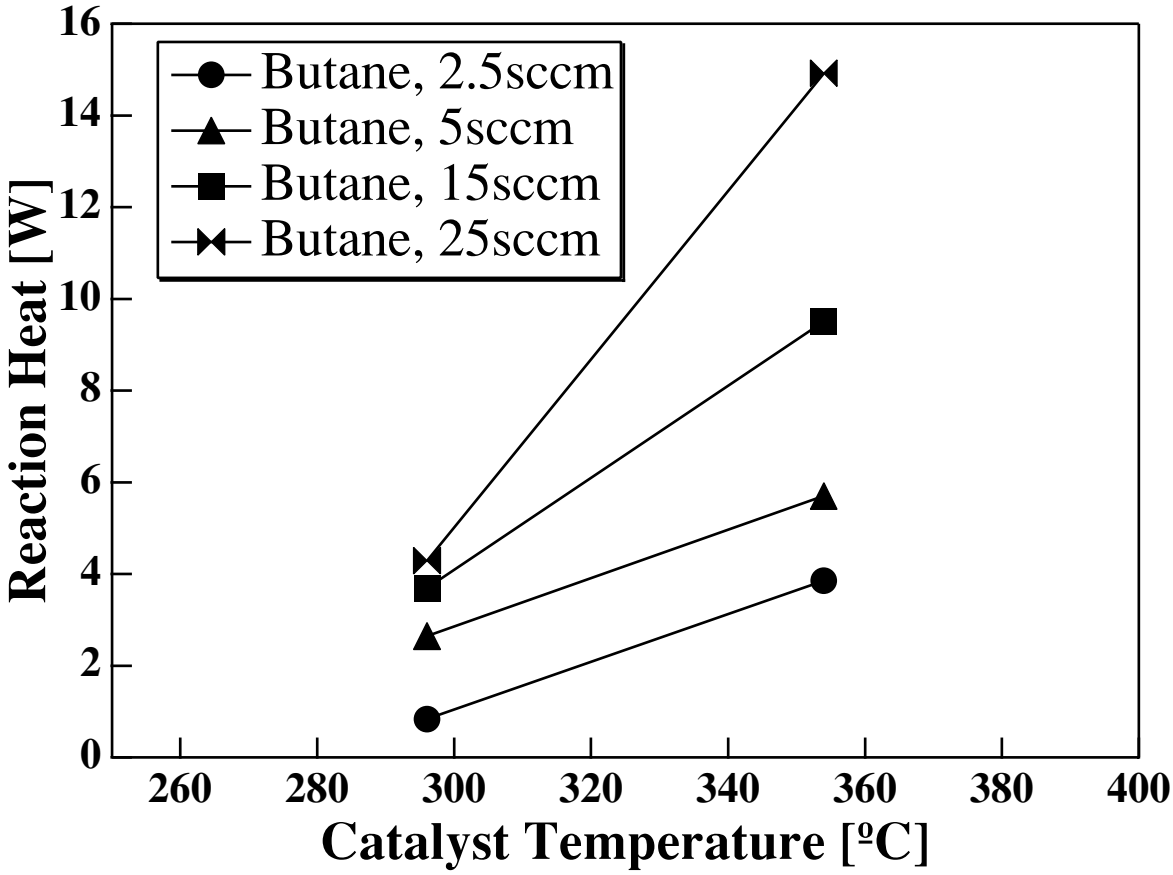

Figure 12 Reaction heat versus catalyst temperature for the Si-based micro catalytic combustor.